Experimental observation of effects of seeds on polymer crystallization

Peng-Wei Zhu,* Andy Phillips, and Graham Edward
Cooperative Research Center (CRC) for Polymers, Department of Materials Engineering, Monash University, Victoria 3800, Australia

Lance Nichols
CRC for Polymers and CSIRO Molecular & Health Technologies, Victoria 3168, Australia

(Received 19 August 2009; published 3 November 2009)

The effects of two seeds on the melt crystallization of isotactic polypropylene were experimentally investigated. The seed, which has the flat surface full of a nonuniform size distribution, has provided a right surface pattern to activate effectively the heterogeneous nucleation. In contrast, the seed, which has the curved surface full of a uniform size distribution, has failed to induce the heterogeneous nucleation. The results from the present work have also shown that the seed with strong nucleating ability leads to the formation of large crystals but the seed without nucleating ability does not influence much the crystal size.

DOI: 10.1103/PhysRevE.80.051801 PACS number(s): 36.20.−r, 81.10.Aj

I. INTRODUCTION

Although there has been a lot of experimental and theoretical work on the heterogeneous crystallization of polymers, this field still attracts much attention due to its intrinsic scientific interest and technological importance [1,2]. The crystallization from a supercooled liquid into a crystalline solid begins with the formation of nuclei. Unlike homogeneous crystallization, which takes place due to a random thermal fluctuation, heterogeneous crystallization is activated through adsorption and wetting, in a repeatable manner, on the surface of foreign particles or seeds. It is generally accepted that the presence of foreign particles enhances crystallization by lowering the free-energy barrier for nucleation by means of the force field near surfaces. However, the force field depends on the surface patterns and geometrical arrangement of seeds.

Recent investigations have greatly advanced our understanding of heterogeneous crystallization [2–7]. It has been reported that the nucleating ability or nucleus stability is influenced by the seed curvature [3,4]. Nuclei attached on curved surfaces are less stable than those on flat surfaces due to the deformation or stress. When nucleus precusors attach onto a highly curved surface, their surfaces cannot accurately match the seed surface [3]. Such nucleus precusors are expected to disintegrate or break up from the seed surface. A seed has nucleating ability only if its size exceeds a well-defined minimum. The free-energy barrier for nucleation is reduced as the curvature of a seed is decreased. In a recent development, however, porous seeds are found to effectively activate the heterogeneous crystallization on curved surfaces [4–7]. It is found that a variety of proteins with radii of 2–5 nm crystallize in the presence of porous seeds with pore radii of 2–10 nm [4,5]. In this case, the protein molecules diffuse into the pores of microporous silicon. This phenomenon has been theoretically rationalized as a consequence of two stages [6,7]. Nucleation actually starts in the corners inside the pores, rather than on the curved surfaces, and when the crystals fully fill the pore space, they break out of the pores and go on to induce the bulk crystallization.

The present work is motivated by the desire to understand the effects of surface pattern and particle geometry on the melt crystallization of semicrystalline polymers. If the surface of a seed is still full of holes or crevices but none of the holes are big enough to allow a whole chain molecule to enter the seed, there could not be nucleation at the corner of pores inside the seed. Most of additives, which have been widely used for the melt crystallization of synthetic polymers have this surface feature [8]. In this case, the particle geometry and/or surface pattern of a seed should play a crucial role in activating the heterogeneous crystallization. A detailed examination along this line however is not available in the literature. In the present work, instead of special additives or agents, two kinds of compound, which have been commonly used are selected as the seeds. It is hoped that the scientific significance drawn from the present work can guide implicitly large scale applications. For the aim of the work, of course, the surface pattern and particle geometry of one seed should be highly distinct from another.

Copper phthalocyanine (CuPc) is a compound which has been intensively used as a blue pigment. It has also been investigated with respect to its optical, magnetic, and electronic conduction properties. Individual CuPc molecules have a planar shape and crystallize into two forms commonly denoted α-crystals and β-crystals [see Fig. 1(a)] [9,10]. The planar molecules are closely packed in parallel with each other along the b-axis to form molecular columns. The intermolecular interactions within the stacks are stronger than those between the stacks. In view of the surface pattern and geometry, CuPc can be regarded as a model seed, which locally has a flat surface full of crevices of nonuniform sizes and which has an anisotropic geometry. These features would be a good template for heterogeneous crystallization [3,4].

The molecular unit of ultramarine blue (UB) is a sphere, which is characterized by a cubo-octahedral cage (often called as β cage) with a sulfur chromophore encapsulated inside [see Fig. 1(b)] [11,12]. UB is also a blue pigment extensively used in many sectors and applications including polymers, detergents, cosmetics, soaps, inks, and papers. The

*Corresponding author.

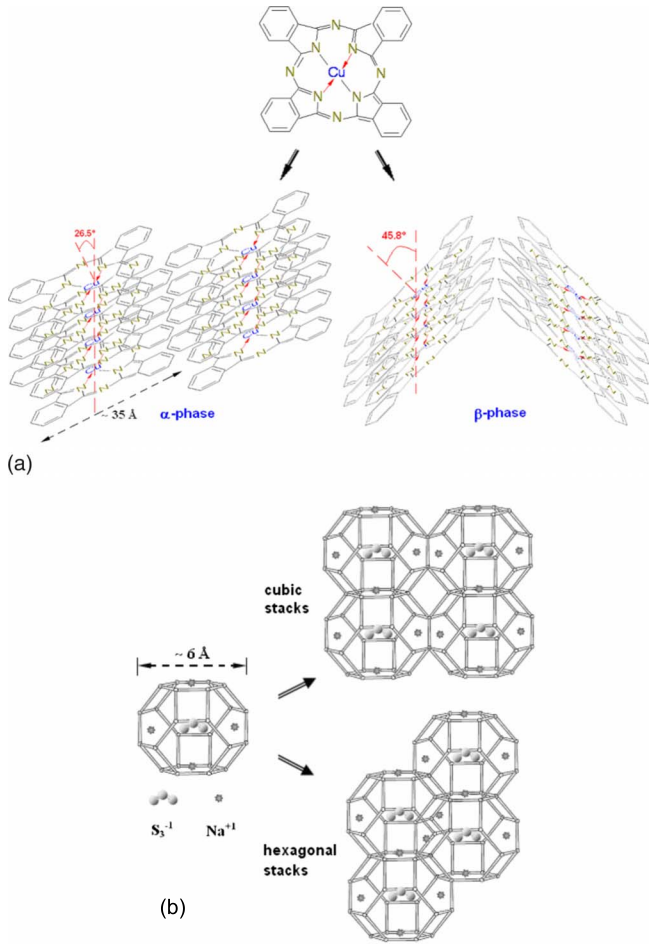

FIG. 1. (Color online) (a) Structures of copper phthalocyanine. (b) Structures of ultramarine blue.

ultramarines usually form a sodalite structure, which is composed of stacked β-cages with a diameter of ~6 Å, connected to eight adjoining cages through six-ring windows with a diameter of ~3 Å [11,12]. In contrast to CuPc, UB is a model seed, which has a curved surface full of the holes of a uniform size and has a locally isotropic geometry. The theoretical model and experiments have suggested that, in general, the curved surface with a uniform size of pore does not favor the heterogeneous crystallization [3,4].

We report the effects of these two seeds on the melt crystallization of isotactic polypropylene (iPP). Based on established kinetic nucleation theory [13], the behavior at different crystallization temperatures can be divided into different regimes. In regime I at the highest temperatures, the rate of lateral spreading is much greater than the rate of nucleation. Accordingly, the absorbed molecules can freely spread by chain folding along the substrate surface before a new nucleation event occurs. In regime III at the lowest temperatures, the rate of nucleation is much greater than the rate of lateral spreading. The adsorbed molecular stems have almost no chance to spread laterally and the majority of stems are deposited on the crystal substrate through the accumulation of nucleation event. Regime II is in a range of intermediate temperatures at which the spreading rate is comparable to the nucleation rate. In this regime, the multiple nuclei form on the substrate before the previous layer is complete. For iPP, the transition from regime II to regime III has been variously reported to be at 137 °C [13] or at 141 °C [14]. In the present work, the crystallization of iPP was carried out in the range of 124–136 °C or in regime III. Since the growth rates of crystallization in regimes I and III are proportional to the surface nucleation rate and have a very similar expression [13], the effect of seeds on the nucleation obtained from regime III, such as the fold surface free energy, can be directly related to that in regime I [13].

II. EXPERIMENTAL DETAILS

A. Materials and sample preparation

An iPP was obtained from Borealis (Borealis HD601CF). The weight and number-molecular weights are 367 000 and 74 000, respectively. The UB and CuPc were obtained from Polypacific Australia and used as received. They were first premixed with iPP in a blender at room temperature and then in a twin screw extruder at 220 °C. The strands extruded were immediately quenched into water and then cut to pellets. The samples were labeled as iPP-0.0, iPP-U0.2, iPP-U0.5, iPP-U0.8, iPP-P0.2, iPP-P0.5, and iPP-P0.8, corresponding to the concentrations of none, 0.2%, 0.5%, and 0.8% by weight, where U and P stand for UB and CuPc, respectively.

B. Isothermal crystallization

The isothermal crystallization was carried out in a Perkin-Elmer Pyris1 differential scanning calorimeter (DSC), and the temperature was calibrated using indium and zinc standards. The samples were sealed in aluminum pans under nitrogen and the typical sample weight was about 6–8 mg. The samples were heated to 210 °C at 30 °C/min and kept at this temperature for 4 min. Then the samples were then cooled to a crystallization temperature T_c at 30 °C/min and kept at T_c for certain times. The heat flow with time was recorded at T_c upon crystallization. The kinetics of isothermal crystallization was analyzed using the Avrami equation [15]:

$$1 - X_{rel}(t) = \frac{\Delta H_{t=\infty} - \Delta H_t}{\Delta H_{t=\infty} - \Delta H_{t=0}} = \exp(-k_A t^n), \qquad (1)$$

where $X_{rel}(t)$ is the relative crystallinity at time t, $\Delta H_{t=\infty}$ and ΔH_t are the crystallization enthalpies on complete crystallization and at t, respectively, k_A is the rate constant, and n is the Avrami index.

In order to evaluate the effect of seeds on the crystallization, an estimation of the fold surface free energy σ_e is needed, which requires the value of equilibrium melting temperature T_m^0. Accordingly, when the crystallization was completed, the samples were heated from T_c to 210 °C at 10 °C/min and the melting temperature T_m was obtained. The T_m^0 was determined from the Hoffman-Weeks plot [16]:

$$T_m = \frac{T_c}{\psi} + T_m^0\left(1 - \frac{1}{\psi}\right), \qquad (2)$$

where ψ is a stability constant. A plot of T_m versus T_c is linear and intersects the line $T_m = T_c$ at T_m^0.

C. Nonisothermal crystallization

Nonisothermal crystallization was carried out at cooling rates of 5, 10, 20, and 30 °C/min. The samples were kept at 210 °C for 4 min before cooling. The activation energy, ΔE, for the entire crystallization was phenomenologically analyzed, in the simplest way, using the Kissinger method [17]:

$$d\left[\ln\left(\frac{\varphi}{T_{c,p}^2}\right)\right] = -\frac{\Delta E}{R} d\left(\frac{1}{T_{c,p}}\right), \tag{3}$$

where ϕ is a cooling rate, $T_{c,p}$ is a peak of crystallization temperature, and R is the gas constant.

D. X-ray characterization

Synchrotron X-ray experiments were carried out at Australian National Beamline Facility (ANBF) in Tsukuba, Japan, and the experimental details can be found in the previous work [18]. In brief, the ANBF is installed on a bending magnet port, and delivers monochromatic synchrotron x-rays in the energy range 4.5–20 keV to the experimental station in a hutch. The instrument has a multiconfiguration vacuum diffractometer that uses image plates as its detector system. The square-shaped beam had a dimension of 200 $\times 200$ μm^2 and the wavelength was 2.0 Å.

The scattered intensity through a hole on a wide-angle x-ray scattering (WAXS) image plate was recorded by a small-angle x-ray scattering (SAXS) image plate. The mass crystallinity X_m determined from WAXS was converted to the volume crystallinity X_V using $(\rho_a/\rho_c)X_m/[1-(1-\rho_a/\rho_c)X_m]$, where $\rho_a=0.845$ and $\rho_c=0.936$ are the densities of amorphous and crystalline phases of iPP, respectively. The intensity of SAXS was integrated and plotted against the scattering vector, $q=(4\pi/\lambda)\sin(\theta)$, where 2θ is the scattering angle. Scattering without a sample, I_b, was subtracted from the measured scattering I_m. The I_m was further corrected by subtracting the thermal density fluctuation, I_t, using a slit-smeared form of modified Porod's law [19].

III. RESULTS AND DISCUSSION

A. Equilibrium melting temperature

Figure 2 shows some typical Hoffman-Weeks plots. The value of T_m^0 is 205 °C for iPP-0.0. In the presence of CuPc seed, the values of T_m^0 are about 179–182 °C, indicating that the CuPc seed significantly decreases T_m^0 of iPP. In the presence of UB seed, the values of T_m^0 of iPP are about 203–205 °C. Apparently, the effect of UB seed on T_m^0 is negligibly small.

B. Isothermal crystallization

Figure 3 shows the time dependence of heat flow during isothermal crystallization. The time dependence of relative crystallinity, X_{rel}, is shown in the insets of Fig. 3. The crystallization time decreases with a decrease in T_c, as generally expected, regardless of the seeds. However, the crystallization time is much shorter in the presence of CuPc seed than that in the presence of UB seed. A comparison can be quantitatively made using the half-time $t_{1/2}$, which is the time for

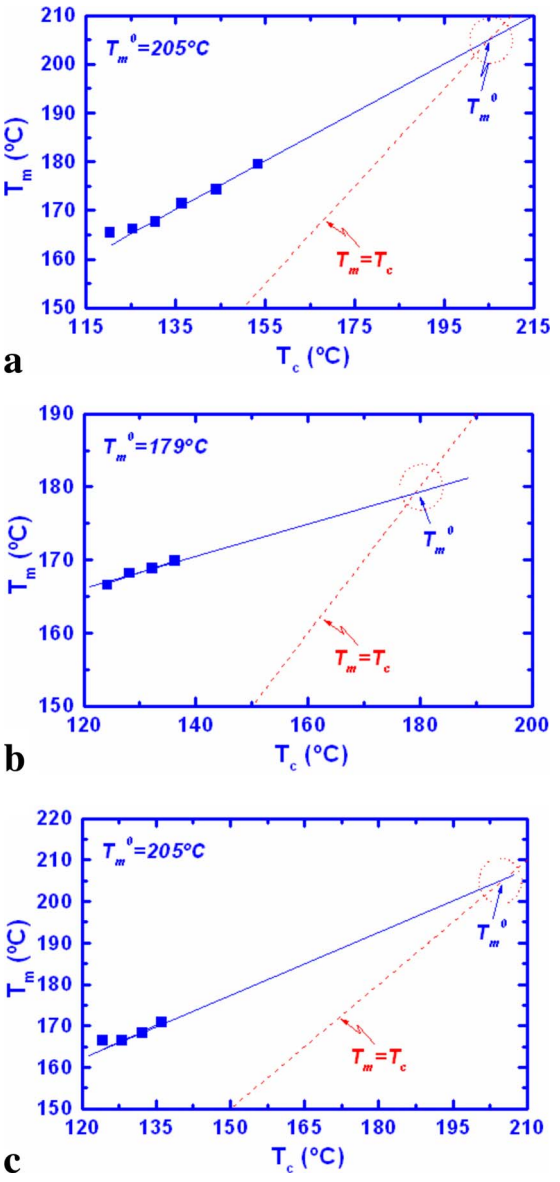

FIG. 2. (Color online) Hoffman-Weeks plots: (a) iPP-0.0, (b) iPP-P0.5, and (c) iPP-U0.5.

50% crystallinity to be achieved. The typical T_c dependence of $t_{1/2}$ is shown in Fig. 4. As can be seen, for example, the $t_{1/2}$ of iPP-P0.8 can be 30 times lower than that of iPP-0.0, whereas the $t_{1/2}$ of iPP-U0.8 is only about 1.4 times lower. Evidently, the CuPc seed provides a much better template for accelerating the entire crystallization process than the UB seed.

Figure 5 shows the Avrami plots of Fig. 3. The Avrami index n was determined from the slope in a plot of $\log[-\ln(1-X_{rel}(t))]$ versus $\log(t)$. The n value of iPP-0.0 is ~4 and almost independent of T_c [see Fig. 5(a)], which is comparable to that reported in the literature [20]. The n is known to relate to the nucleation mechanism and growth geometry of crystals [21]. The results indicate that the iPP-0.0 undergoes spherulitic growth or homogeneous crystallization.

In the presence of CuPc seed, n becomes T_c dependent [see Fig. 5(b)]. Especially, n is reduced remarkably as T_c is

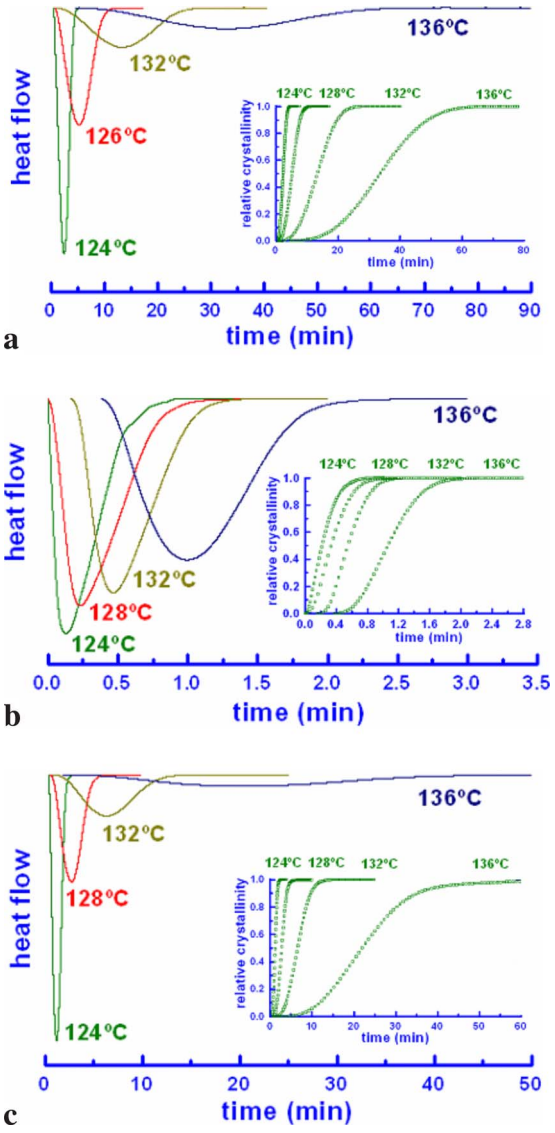

FIG. 3. (Color online) Time dependence of heat flow during isothermal crystallization at different crystallization temperatures T_c and time dependence of relative crystallinity X_{rel}: (a) iPP-0.0, (b) iPP-P0.8, and (c) iPP-U0.8.

decreased. The n value of iPP-P0.8 is 3.4 at 136 °C and 2.8 at 132 °C, and it is decreased further to 1.9 at 128 °C to 1.6 at 124 °C. For heterogeneous crystallization, n values of 3 and 2 suggest a spherulitic growth and a disk-like growth, respectively [20,21]. Accordingly, at 132 and 136 °C, the crystallization from already existing nuclei is a three-dimensional growth. At 124 and 128 °C, the crystallization approaches a two-dimensional (2D) growth. Note that the decrease in $t_{1/2}$ with T_c is accompanied by a decrease in n [see Figs. 4 and 5(b)].

In the presence of UB seed, n values of iPP-U0.8 are in a good agreement with those of iPP-0.0 [see Fig. 5(c)]. From the view of n or the growth geometry, these results seem to indicate that the crystallization proceeds as if it were from the homogeneous nucleation. If we consider $t_{1/2}$, however, we can see that the entire crystallization of iPP-U0.8 is still accelerated, though not dramatically.

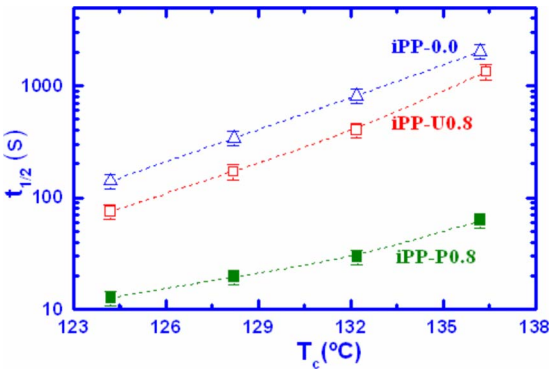

FIG. 4. (Color online) Plots of half time $t_{1/2}$ of crystallization versus crystallization temperature T_c for iPP-0.0, iPP-P0.8, and iPP-U0.8.

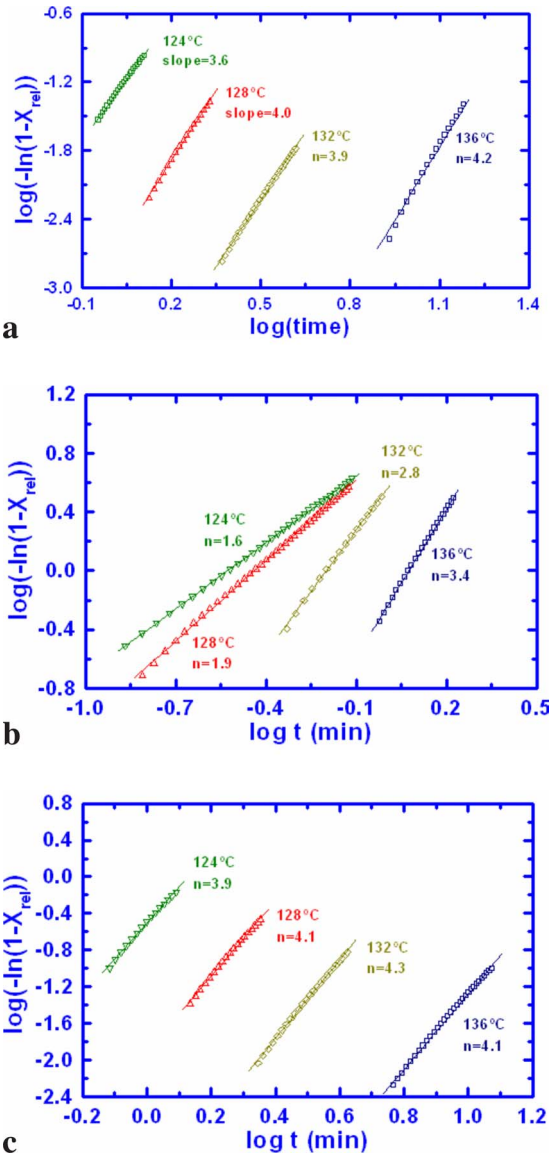

FIG. 5. (Color online) Avrami plots at different crystallization temperatures T_c: (a) iPP-0.0, (b) iPP-P0.8, and (c) iPP-U0.8.

It is worth noting that the smaller value of Avrami index n is associated with a confined crystallization [22–24]. The effects of confinement on polymer crystallization have been investigated for the systems such as polymers inside pores and block copolymers in microdomains [22,23]. In the present work, the confined crystallization occurs on the flat surface at the lower T_c (n=1.6 and 1.9) but the confinement is released at the higher T_c (n=2.8 and 3.4). The confinement is not triggered by the curved surface at any T_c. The flat surface would provide the greater chance to absorb molecular stems and effectively stabilize these absorbed segments.

C. Fold chain free energy

The above results have revealed that the effects of the seeds on the rate of entire crystallization (half time $t_{1/2}$) and the growth dimension (Avrami index n) at different T_c. The entire crystallization is known to include contributions from both nucleation and growth. Nucleation in general is the crucial stage that determines the entire crystallization process. The effects of the seeds on the energy barrier for the fold surface energy are evaluated.

According to the surface nucleation theory of Lauritzen and Hoffman (LH), the growth rate of polymer crystals at T_c, $G(T_c)$, can be given as follows [13,25]:

$$G(T_c) = G_0 \exp\left[-\frac{U^*}{R(T_c - T_\infty)}\right]\exp\left[-\frac{K_g}{T_c(T_m^0 - T_c)f}\right], \tag{4}$$

where G_0 is a growth rate constant, U^* is a "universal" constant related to the transport of molecules across the interfacial boundary between melt and crystal. T_∞ is a temperature at which all the motions associated with the viscous flow cease, f is a correcting factor for variation in heat with temperature and is approximated by $f=2T_c/(T_m^0+T_c)$, and K_g is a nucleation constant related to the energy barrier for the formation of a critical nucleus. The growth rate $G(T_c)$ is inversely proportional to the half time $t_{1/2}(T_c)$ [22,26]. The U^* is 6270 J/mol according to the literature [25]. T_∞ is defined as $T_\infty = T_g - 30$ K, where T_g is the glass transition temperature (263 K for iPP [27]).

The K_g can be obtained from the slope in a plot of $[\ln(1/t_{1/2}) + U^*/R(T_c - T_\infty)]$ versus $1/[T_c(T_m^0 - T_c)f]$ (see Fig. 6). The concentration dependence of K_g is given in Fig. 7(a). The fold chain free energy σ_e can be calculated from K_g defined as follows [13,25]:

$$K_g = \frac{j\sigma\sigma_e b_0 T_m^0}{k\Delta H}, \tag{5}$$

where σ is the lateral surface free energy, b_0 is the thickness of a monolayer, k is the Boltzmann constant, and ΔH is the heat of fusion. For iPP, σ=11.5 J/cm^2, b_0=6.26 Å, and ΔH=196 J/cm^3 [14,27]. The value of j depends on the regime, i.e., j is 2 for the regime II and 4 in the regimes I and III (which is the case in the present work). Figure 7(b) displays the concentration dependence of σ_e.

K_g and σ_e values are $\sim 7.1\times 10^5$ K^2 and $\sim$0.141 J/m^2 for iPP-0.0, respectively. The results are comparable to those

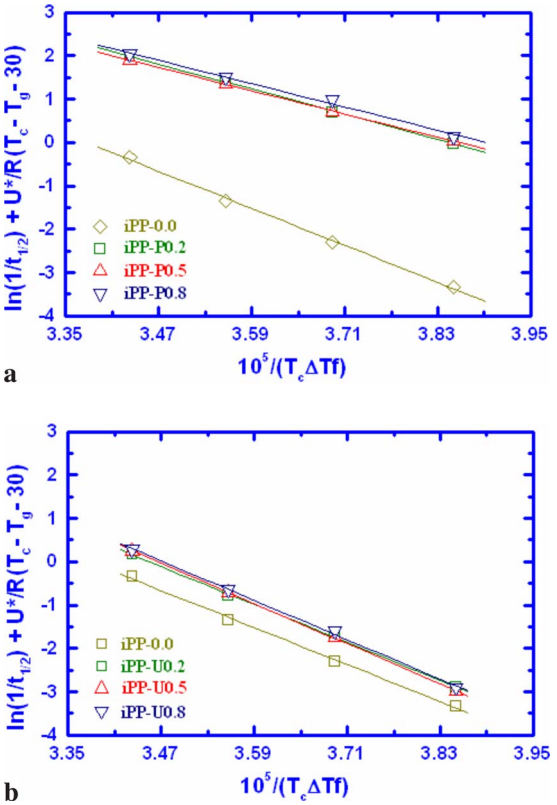

FIG. 6. (Color online) Hoffman-Lauritzen plots: (a) samples containing CuPc seed and (b) samples containing UB seed.

reported in the literature [21]. In the presence of CuPc seed, the σ_e is decreased to $\sim$0.095 J/m^2 for iPP-P0.2 and further to $\sim$0.088 J/m^2 both for iPP-P0.5 and for iPP-0.8, respectively. In the presence of UB seed, however, the σ_e values are about 0.144–0.151 J/m^2, indicating that the σ_e is almost a constant, or if at all, slightly increases with seed content. Apparently, the present work has shown that the presence of foreign particles does not necessarily lower the free-energy barrier for nucleation. The particle geometry and surface pattern can effectively affect the heterogeneous nucleation [3,7].

In the present work, the flat surface full of nonuniform size crevices has proved to be an effective template for nucleation, whereas the curved surface full of a uniform size of holes has failed. The observation that the entire crystallization is accelerated in the presence of CuPc seed (see Figs. 3 and 4) is attributed to the lower free-energy barrier for the nucleation. This can be explained as the more and stable absorbed molecular stems on the flat surface [3]. The nonuniform sizes of crevices would also provide the greater chances for heterogeneous nucleation. Our results experimentally support the theoretical predictions and computer simulations [2,3].

D. Activation energy for crystallization

The LH theory has successfully predicted the undercooling dependence of growth rate, the regime transition behavior, and the undercooling dependence of thickness of crystalline lamellae [25]. The theory considers the free energy

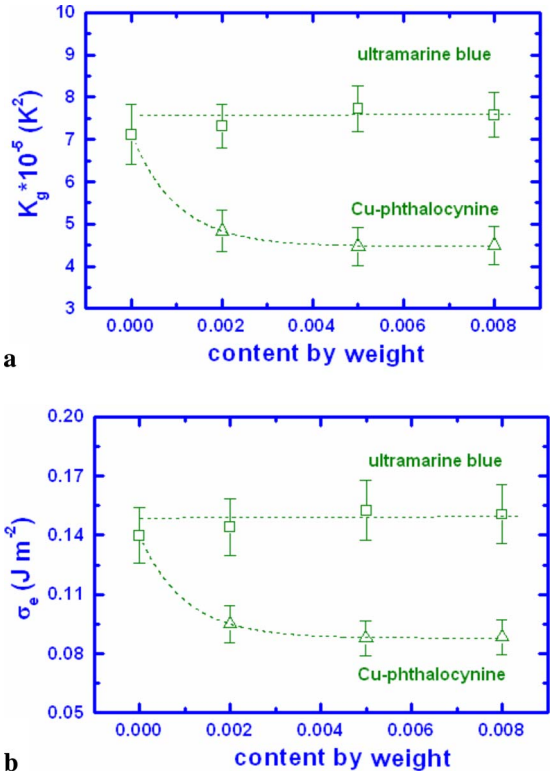

FIG. 7. (Color online) (a) Seed concentration dependence of nucleation constant K_g. (b) Seed concentration dependence of fold surface free energy σ_e.

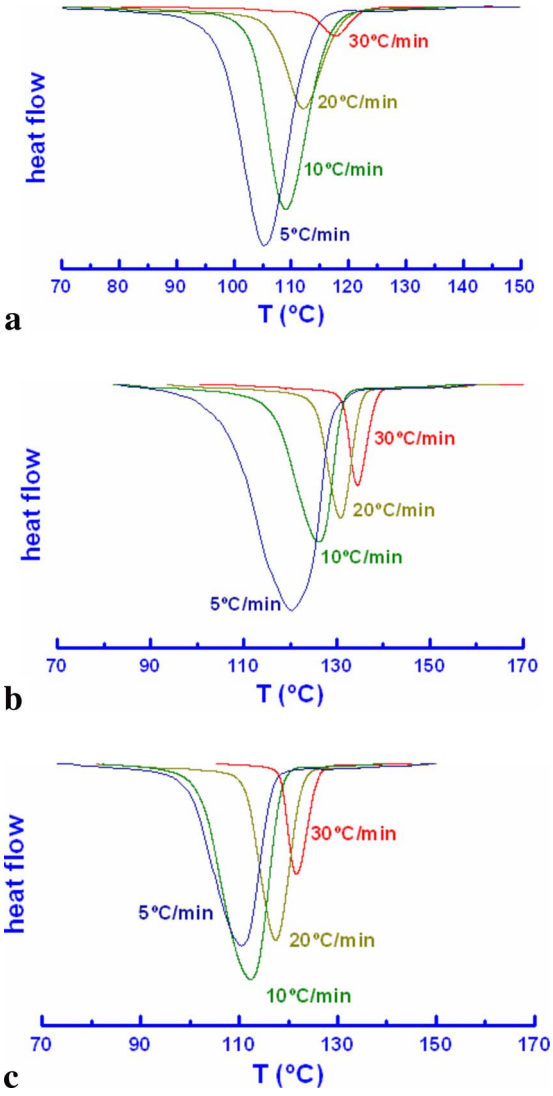

FIG. 8. (Color online) Temperature dependence of heat flow at different cooling rates ϕ during nonisothermal crystallization: (a) iPP-0.0, (b) iPP-P0.8, and (c) iPP-U0.8.

difference between the states before and after deposition of molecular stems. In order to understand further the effect of the seeds on the entire crystallization, the apparent activation energy, ΔE, for the crystallization was also evaluated. This is particularly relevant to the UB seed. As has been seen, the UB does not activate the heterogeneous nucleation but its presence does speed up, though not dramatically, the entire crystallization (see $t_{1/2}$ in Fig. 4).

Figure 8 shows the temperature dependence of heat flow during the nonisothermal crystallization. ΔE was then calculated from Fig. 8 using the Kissinger method [see Eq. (3)] [17]. The results are displayed in Fig. 9. ΔE here is phenomenologically interpreted as an apparent energy barrier for all the events participating in the crystallization including the diffusion of chain molecules toward the nucleation sites. ΔE value is ~225 kJ/mol for iPP-0.0, which is comparable to that reported in the literature [27]. It is found that ΔE values are ~176 and ~199 kJ/mol for iPP-P0.8 and iPP-U0.8, respectively. The shorter $t_{1/2}$ of iPP-U0.8 (though only 1.4 times lower) can be rationalized as the lower ΔE, although the UB seed does make a difference in the nucleation. As for the CuPc seed, in addition to the smaller σ_e, the shorter $t_{1/2}$ of iPP-P0.8 (30 times lower) is also related to the lower ΔE. This observation may be an individual case related to the plasticization of UB particles but the detailed mechanism underlying the observation is not clear. It is worth noting that the reverse phenomenon was experimentally observed; i.e., additives cause the lower σ_e but the higher ΔE for the melt crystallization of iPP [27].

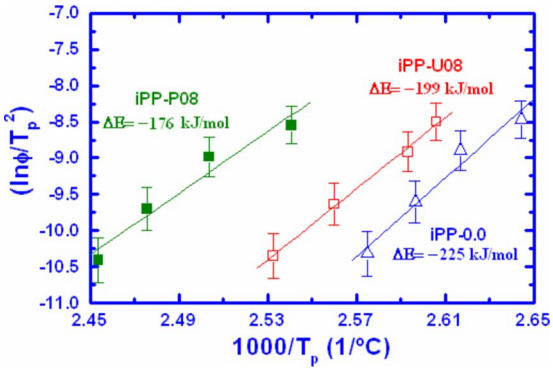

FIG. 9. (Color online) Kissinger plots of iPP-0.0, iPP-P0.8, and iPP-U0.8.

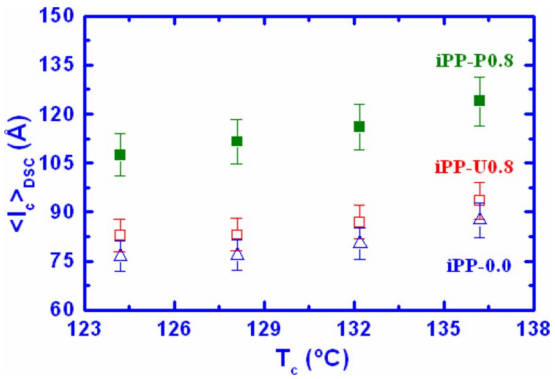

FIG. 10. (Color online) Plots of thickness of crystalline lamellae $\langle l_c \rangle_{DSC}$ versus crystallization temperature T_c for iPP-0.0, iPP-P0.8, and iPP-U0.8.

E. Morphology

The average thickness of crystalline lamellae, denoted as $\langle l_c \rangle_{DSC}$, was estimated from the DSC data using the Thomson-Gibbs equation [25]:

$$\langle l_c \rangle_{DSC} = \frac{2\sigma_e T_m^0}{\Delta H (T_m^0 - T_m)}. \tag{6}$$

As can be seen from Fig. 10, the presence of CuPc seed significantly increases $\langle l_c \rangle_{DSC}$ or crystal size. For example, at $T_c = 136$ °C, $\langle l_c \rangle_{DSC}$ is increased from ~88 Å of iPP-0.0 to ~124 Å of iPP-P0.8. By comparison, the presence of UB seed can only lead to a small increase in the crystal size. The results are apparently related to the balance between σ_e and $(T_m^0 - T_m)$. It should be pointed out that the use of DSC as a tool to determine the thickness of crystalline lamellae is very sensitive to the heating rate [28]. The observation from the DSC experiments should be further confirmed using WAXS and SAXS as comparison tools.

Figure 11 shows 2D WAXS image patterns and one-dimensional (1D) profiles that were obtained from circularly integrated intensities of 2D patterns. The samples used for the X-ray experiments were crystallized at 150 °C. iPP is of polymorphic composition with three crystal structures, i.e., monoclinic α-crystal, hexagonal β-crystal, and orthorhombic γ-crystal [29]. The quiescence crystallization of iPP at 150 °C only results in the formation of α-crystal. The main reflection peaks corresponding to the α-crystal are given in Fig. 11. The degrees of volume crystallinity, X_v, are 0.53, 0.58, and 0.66, respectively, for iPP-0.0, iPP-U0.8, and iPP-P0.8. In addition to the crystallinity, the crystallite size can be estimated from the WAXS reflections using the Scherrer equation [30]. Since there is the absence of a pure reflection from $(00l)$ in iPP, the crystal size along the c-axis, d_{001}, was calculated from the reflection $(\bar{1}31)$ using the following equation [18]:

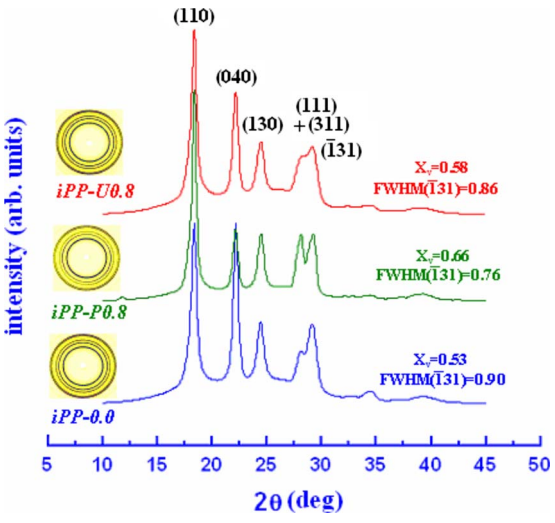

FIG. 11. (Color online) 2D WAXS image patterns and corresponding 1D profiles from iPP-0.0, iPP-P0.8, and iPP-U0.8.

$$d_{001} = d_{\bar{1}31} \cos\varphi = \frac{K\lambda}{\omega_{\bar{1}31} \cos\vartheta_{\bar{1}31}} \cos\varphi \tag{7}$$

where $\varphi = 57.89°$ is an angle between (001) and $(\bar{1}31)$ planes, K is a crystallite shape factor, and $\omega_{\bar{1}31} = (B_{\bar{1}31}^2 - B_0^2)^{1/2}$ with $B_{\bar{1}31}$ being a full width at half-maximum (FWHM) intensity and B_0 the instrumental resolution. The values of d_{001} along the c-axis are 71, 73, and 85 Å for iPP-0.0, iPP-U0.8, and iPP-P0.8, respectively.

Figure 12(a) shows 2D SAXS image patterns and 1D Lorentz-corrected profiles. The average long spacing, $\langle L \rangle_{CF}$, can be calculated from a one-dimension correlation function $\gamma(z)$ [31,32]:

$$\gamma(z) = \frac{\int_0^\infty [I_m(q) - I_t - I_b(q)] q^2 \cos(qz) dq}{\int_0^\infty [I_m(q) - I_t - I_b(q)] q^2 dq}. \tag{8}$$

The SAXS data were extrapolated to $q \to 0$ according to the Guinier model and to $q \to \infty$ according to the Porod's law. The values of $\langle L \rangle_{CF}$ are 82, 90, and 156 Å, respectively, for iPP-0.0, iPP-U0.8, and iPP-P0.8 [see Fig. 12(b)]. The analysis of $\gamma(z)$ also gave the average thickness of crystalline lamellae, denoted as $\langle l_c \rangle_{CF}$. The values of $\langle l_c \rangle_{CF}$ are 64, 67, and 127 Å for iPP-0.0, iPP-U0.8, and iPP-P0.8, respectively.

Apparently, both WAXS and SAXS results have clearly shown that the CuPc seed significantly increases the thickness of crystalline lamellae or crystal sizes whereas the UB seed is not an effective crystal grower. The trend is consistent with that observed from the DSC experiments, although the values of thickness, as expected, are different from the different methods.

In addition, the FWHM of Lorentz-corrected SAXS peaks [see inset of Fig. 12(a)] can be used as a measure of homogeneity of lamellar distribution [33]. The values of FWHM are 0.032, 0.028, and 0.008 for iPP-0.0, iPP-U0.8, and iPP-P0.8, respectively. The smaller FWHM is related to the narrower distribution of crystalline lamellae. In this sense, the results imply that the CuPc seed is also able to tune the preferred orientation even in the quiescent crystallization.

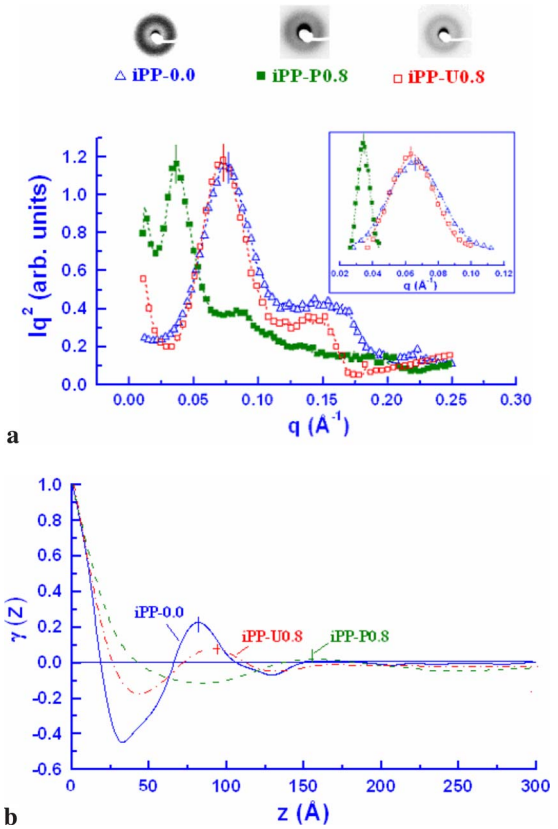

FIG. 12. (Color online) (a) 2D SAXS image patterns and corresponding 1D Lorentz-corrected profiles from iPP-0.0, iPP-P0.8, and iPP-U0.8. (b) Correlation function profiles obtained from (a).

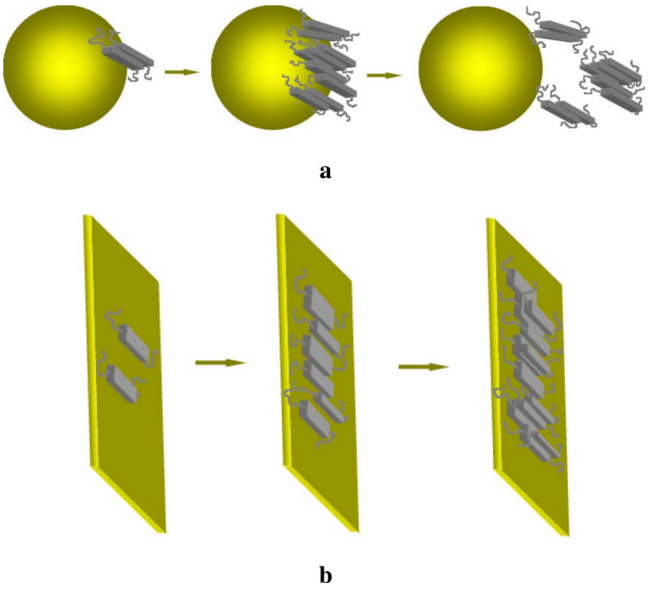

FIG. 13. (Color online) Schematic mechanisms for growth of nuclei or deposition of stems on seeds: (a) curved surfaces and (b) flat surfaces. Precusors of nuclei attached on curved surfaces are less stable than those on flat surfaces due to the deformation or stress. They can break from curved surfaces before they grow to a critical size, as shown in (a). As a result, a critical nucleus forms only in the bulk even in the presence of spherical seeds.

The surface features of CuPc seed, including flatness, size diversity, and size distribution, would concentrate the contacts between segments and surfaces, direct the preferential wetting of chains, and stabilize the molecular stems on deposition. All these favor the orientation of polymer crystals.

IV. CONCLUSIONS

The effects of the seeds on the quiescent crystallization of iPP were experimentally investigated. The two seeds have different particle geometries and surface patterns but have in common small sizes of holes on the surfaces. The seed with the flat surface full of nonuniform size distribution has proved to be a very effective nucleant. In contrast, the seed with curved surface full of a uniform size distribution has failed to facilitate the heterogeneous nucleation. It is suggested that the surface curvature plays a dominant role in controlling the nucleation, although the effects of surface holes and crevices on the nucleation cannot be totally ruled out. The influence of surface curvature on the formation of nuclei is schematically illustrated in Fig. 13. The results have also shown that the seed with strong nucleating ability provides a good template for the formation of larger crystals but the seed without nucleating ability does not influence much the crystal size. The present work is an example of exploring experimentally the effect of seeds on the heterogeneous crystallization. The melt crystallization of semicrystalline polymers would be another class of substances for establishing the "universality" of theories [2–7]. The results can help us to design and select suitable nucleants for controlling crystallization and morphology.

ACKNOWLEDGMENT

The part of this work was performed at the Australian National Beamline Facility (ANBF) with support from the Australian Synchrotron Research Program, which is funded by the Commonwealth of Australia under the Major National Research Facilities Program. P.-W. Zhu gratefully acknowledges Daan Frenkel and Mitsuyoshi Fujiyama for helpful comments and discussion.

[1] M. Muthukumar, Adv. Chem. Phys. **128**, 1 (2003).
[2] R. P. Sear, J. Phys.: Condens. Matter **19**, 033101 (2007).
[3] A. Cacciuto, S. Auer, and D. Frenkel, Nature (London) **428**, 404 (2004).
[4] N. E. Chayen, E. Saridakis, and R. P. Sear, Proc. Natl. Acad. Sci. U.S.A. **103**, 597 (2006).
[5] N. E. Chayen, E. Saridakis, R. El-Bahar, and Y. Nemirovsky, J. Mol. Biol. **312**, 591 (2001).

[6] A. J. Page and R. P. Sear, Phys. Rev. Lett. **97**, 065701 (2006).
[7] D. Frenkel, Nature (London) **443**, 641 (2006).
[8] J. Kurja and N. A. Mehl, *Plastics Additive Handbook* (Hanser, Munich, 2001).
[9] J. R. Fryer, J. Porphyr. Phthalocyanines **3**, 672 (1999).
[10] J. R. Fryer, J. Electron Microsc. Tech. **11**, 310 (1989).
[11] D. Arieli, D. E. W. Vaughan, and D. Goldfarb, J. Am. Chem. Soc. **126**, 5776 (2004).
[12] N. Gobeltz-Hautecoeur, A. Demortier, B. Lede, J. P. Lelieur, and C. Duhayon, Inorg. Chem. **41**, 2848 (2002).
[13] E. J. Clark and J. D. Hoffman, Macromolecules **17**, 878 (1984).
[14] Y. F. Wang and D. R. Lloyd, Polymer **34**, 2324 (1993).
[15] M. Avrami, J. Chem. Phys. **7**, 1103 (1939).
[16] J. Hoffman and J. Weeks, J. Res. Natl. Bur. Stand. **A66**, 13 (1962).
[17] H. E. Kissinger, J. Res. Natl. Bur. Stand. **57**, 217 (1956).
[18] P. W. Zhu, J. Tung, A. Phillips, and G. Edward, Macromolecules **39**, 1821 (2006).
[19] J. Koberstein and R. S. Stein, J. Polym. Sci., Polym. Phys. Ed. **21**, 2181 (1983).
[20] K. R. Reddy, K. Kashiro, T. Sakurai, and N. Yamaguchi, Macromolecules **42**, 1672 (2009).
[21] B. Wunderlich, *Macromolecular Physics* (Academic Press, New York, 1976), Vol. 2.
[22] E. Woo, J. Huh, Y. G. Jeong, and K. Shin, Phys. Rev. Lett. **98**, 136103 (2007).
[23] Y.-L. Loo, R. Register, and A. J. Ryan, Macromolecules **35**, 2365 (2002).
[24] A. Henschel, P. Huber, and K. Knorr, Phys. Rev. E **77**, 042602 (2008).
[25] J. D. Hoffman, D. T. Davis, and J. I. Lauritzen, in *Treatise on Solid State Chemistry*, edited by N. B. Hannay (Plenum Press, New York, 1976), Chap. 7.
[26] C. Angelloz, R. Fulchiron, A. Douillard, B. Chabert, R. Fillit, A. Vautrin, and L. David, Macromolecules **33**, 4138 (2000).
[27] Y. Zhang and Z. Xin, J. Appl. Polym. Sci. **101**, 3307 (2006).
[28] H. Zhou and G. L. Wilkes, Polymer **38**, 5735 (1997).
[29] J. Brandrup and E. H. Immergut, *Polymer Handbook* (Wiley, New York, 1989).
[30] L. E. Alexander, *X-ray Diffraction Methods in Polymer Science* (Wiley, New York, 1969).
[31] G. R. Strobl, *The Physics of Polymers* (Springer, New York, 1997).
[32] F. J. Balta-Calleja and G. G. Vonk, *X-ray Scattering of Synthetic Polymers* (Elsevier Science, New York, 1989).
[33] Y. W. Cheung, R. S. Stein, J. S. Lin, and G. D. Wignall, Macromolecules **27**, 2520 (1994).